Mathematical Biology

Deformations of acid-mediated invasive tumors in a model with Allee effect

Paul Carter[1] · **Arjen Doelman**[2] · **Peter van Heijster**[3] · **Daniel Levy**[4] · **Philip Maini**[5] · **Erin Okey**[6] · **Paige Yeung**[7]

© The Author(s) 2025

Abstract

We consider a Gatenby–Gawlinski-type model of invasive tumors in the presence of an Allee effect. We describe the construction of bistable one-dimensional traveling fronts using singular perturbation techniques in different parameter regimes corresponding to tumor interfaces with, or without, an acellular gap. By extending the front as a planar interface, we perform a stability analysis to long wavelength perturbations transverse to the direction of front propagation and derive a simple stability criterion for the front in two spatial dimensions. In particular we find that in general the presence of the acellular gap indicates transversal instability of the associated planar front, which can lead to complex interfacial dynamics such as the development of finger-like protrusions and/or different invasion speeds.

1 Introduction

Evolving cancerous tumors go through several phases. Tumors initially appear as relatively small congregations of cells that have undergone genetic mutations that typically cause the tumor to grow at an abnormally high rate (Wodarz and Komarova 2014).

✉ Paul Carter
     pacarter@uci.edu

[1] Department of Mathematics, University of California, Irvine, CA, USA

[2] Mathematical Institute, Leiden University, Leiden, Netherlands

[3] Mathematical and Statistical Methods-Biometris, Wageningen University & Research, Wageningen, Netherlands

[4] Program in Applied and Computational Mathematics, Princeton University, Princeton, USA

[5] Mathematical Institute, University of Oxford, Oxford, UK

[6] Division of Applied Mathematics, Brown University, Providence, RI, USA

[7] Massachusetts Institute of Technology, Cambridge, USA

At onset, this growth is regular and sustained by nutrients, etc., that are transported to the tumor by the governing local diffusion processes. However, at a certain stage, this regular mechanism is no longer able to drive the tumor growth process and the tumor enters the next phase in which it invades the surrounding, healthy, tissue. This stage is characterized by a deformation of the surface of the original clump of (tumorous) cells. The nature of the resulting morphology can determine the invasive capacity, and therefore the overall severity, of the tumor. To invade tissue, tumor cells need to overcome the physical barriers of normal cells and extracellular matrix (ECM), the matrix that provides a physical scaffolding for cells. Understanding how tumor cells achieve this is of obvious importance, especially since at the next stage of the process—known as metastasis—the invading surface of the preceding stage may break away from the primary tumor and invade other parts of body to form, often fatal, secondary tumors.

There are many ways to model the multi-scale process of tumor growth and invasion mathematically, ranging from fully discrete to continuum models, and various hybrid models in between—see for instance Anderson and Quaranta (2008); Lowengrub et al. (2010); Turner and Sherratt (2002). Here, we take the continuum point of view and focus on (generalized, nonlinear) reaction-diffusion type models. Several of these models address the role of matrix metalloproteinases (MMPs), which are enzymes secreted by tumor cells that degrade ECM. For example, Perumpanani et al. (1996) proposed a model consisting of six coupled partial differential equations (PDEs) for cell, ECM and MMP densities, where there are cells of different types (phenotypes) and movement is via the process of haptotaxis (movement up adhesive gradients) as well as diffusion. They analysed, in one spatial dimension, the traveling wave behavior of this system, exploring how the wave speed depends on various cell properties. More recently, Katsaounis et al. (2024) developed a hybrid multiscale 3D model employing PDEs and stochastic differential equations in which cell diffusion is modelled nonlinearly. They carry out a numerical study of the system in the context of a number of biologically motivated case studies. In 1996, Gatenby and Gawlinski (1996) published their seminal paper in which they stated their acid-mediated invasion hypothesis. Namely, they proposed that tumor cells, undergoing glycolysis, which produces lactic acid, could invade normal cells due to the acid being more toxic to normal cells than to tumor cells. Their PDE model was composed of three coupled equations, with a cross-dependent degenerate diffusion term for tumor cell movement. This led to the formation of sharp interfaces representing the surface of the growing tumor and the prediction that, in certain cases, an acellular gap would appear between the tumor and normal cell populations. This prediction was validated in the context of head and neck cancer. This model has been extended in a number of studies to account also for ECM degradation (see, for example, Martin et al. 2010, Strobl et al. 2020).

The mathematical challenges raised by the nonlinear cross-dependent diffusion term in Gatenby and Gawlinski (1996) have inspired many mathematical studies of the traveling wave behavior of this system in one spatial dimension (see Davis et al. 2022; Fasano et al. 2009; Gallay and Mascia 2022 and the references therein). However, these in essence one-dimensional interfaces can only be expected to be stable—and thus observable—in the initial 'regular' stage of tumor growth. In the follow-up phase in which the tumor starts to invade the surrounding tissue, the interface most likely will evolve into a structure with a two- or three-dimensional nature. Viewing such
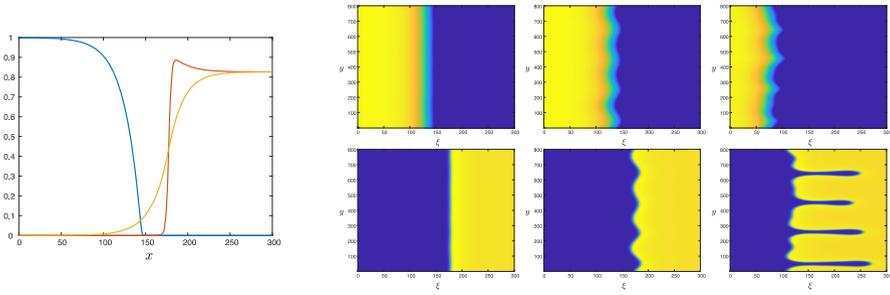
Fig. 1 Results of a direct numerical simulation of (1.1) exhibiting the transversal long wavelength instability for parameter values taken from Gatenby and Gawlinski (1996) $(a, \kappa, \delta_1, \delta_2, \delta_3, \rho, \varepsilon) = (0.35, 0.1, 12.5, 0.1, 70.0, 1.0, 0.0063)$. In the left panel, the underlying (longitudinally stable) one-dimensional traveling wave is shown (in which the normal cell density U is plotted in blue, the tumor cell density V in red, and the acid concentration W in yellow. The six right panels depict the results of two-dimensional simulations. The initial conditions of the two-dimensional run were constructed by trivially extending this 1D-stable profile in the y-direction and adding a small amount of noise. The simulations were performed in a co-moving frame $\xi = x + ct$; in the laboratory frame the tumor would travel with speed $c = 0.0401$ to the left, corresponding to the wave speed of the initial front profile (so that in the absence of any instability, the fronts would appear stationary). The corresponding tumor U-profiles (top three panels) and V-profiles (bottom three panels) are plotted (for $t = 20000, 30000, 40000$ from left to right); for all profiles yellow indicates high density of cells, and blue depicts low density of cells

shapes as possibly arising from a spatial patterning instability, but departing from the idea of a (growing) tumor surface governed by traveling waves, Chaplain et al. (2001) proposed a Turing-type model composed of growth activating and growth inhibiting chemicals and showed how these gave rise to spatial patterns on a spherical surface which, they proposed, would induce 'columnar outgrowths of invading cancer cells'. In this paper, we propose a different mechanism for the formation of outgrowths of invading tumor cells that is based on the tumor surface as the interface between tumorous and healthy tissue governed by bistable traveling fronts (see Fig. 1). Namely, we analyse front evolution—or interface dynamics—in a slightly modified form of the Gatenby-Gawlinski (1996) model to explore the potential appearance of transversal instabilities on interfaces that are longitudinally stable. In other words, we consider two-dimensional fronts for which the underlying one-dimensional traveling waves are stable in the direction of propagation, but for which instabilities may form in directions transversal to this direction. In Fig. 1 we show the outcome of a simulation of the (slightly modified) Gatenby-Gawlinski model in two space dimensions that indeed exhibits such a transversal instability: the interface develops 'fingers' similar to the phenomenon of viscous fingering in fluid dynamics. We emphasize that the instability develops purely due to extending the (longitudinally stable) front as an interface in two spatial dimensions, in the absence of any deterministic or stochastic forcing or inhomogeneity.

In our modified version of the Gatenby-Gawlinski model (Gatenby and Gawlinski 1996), we assume that tumor cells are not fully resistant to lactic acid by including a death term in the tumor cell equation. We also regularise the nonlinear diffusion term by assuming that normal cells do not form an impenetrable barrier to tumor cell invasion. While we do this primarily for mathematical convenience, it should be

noted that there is a biological justification for this as some tumor cells upregulate the expression of aquaporins (see the review Verkman et al. 2008) which, it has been hypothesised, may allow cells to 'bulldoze' their way through surrounding cells and tissues (McLennan et al. 2020). Lastly, we replace the logistic growth term for cancer cells by a term that allows for the Allee effect, which has been proposed to play a role in cancer tumor growth dynamics similar to in ecosystems—see Gerlee et al. (2022); Johnson et al. (2019); Korolev et al. (2014); Sewalt et al. (2016) and the references therein. Thus, we consider the following reaction-diffusion model for tumor invasion,

$$
\begin{aligned}
U_\tau &= U(1 - U) - \delta_1 U W\,, \\
V_\tau &= \rho V(1 - V)(V - a) - \delta_2 V W + \nabla \cdot ((1 + \kappa - U)\nabla V)\,, \\
W_\tau &= \delta_3(V - W) + \frac{1}{\varepsilon^2}\Delta W\,,
\end{aligned}
\tag{1.1}
$$

where $(U, V, W)(x, y, \tau)$ represent normal cell density, tumor cell density, and acid (concentration) produced by the tumor cells, respectively, at spatial position $(x, y) \in \mathbb{R}^2$ and time $\tau \in \mathbb{R}^+$. The parameter δ_1 measures the destructive influence of acid on healthy tissue and can thus be seen as an indicator of tumor aggressivity, the new parameter δ_2 represents the impact of acid on the tumor itself and we assume that $0 \le \delta_2 < \delta_1$, i.e. the effect of W on V is less than that of W on U (but not necessarily zero). The parameter $\rho > 0$ measures the relative production rate of tumor cells compared to healthy cells and $0 < a < 1$ the relative strength of the Allee effect. Since the diffusive spreading speed of acid is much faster than that of cells (Gatenby and Gawlinski 1996) it follows that $0 < \varepsilon \ll 1$ so that reaction-diffusion system (1.1) is singularly perturbed. Finally, the parameter κ measures the regularized nonlinear diffusion effect and is assumed to satisfy $0 < \varepsilon \ll \kappa \ll 1$.

In the spirit of Korolev et al. (2014), the present paper was motivated by recent progress on the formation of invasive, 'fingering', interface patterns as in Fig. 1 in the context of coexistence patterns (between grasslands and bare soil) in dryland ecosystems (Carter 2024; Carter et al. 2023; Fernandez-Oto et al. 2019). In fact, in Carter (2024) and Carter et al. (2023) criteria have been developed by which the transversal (in)stability of planar interfaces in a general class of singularly perturbed two-component reaction-diffusion equations—that includes typical dryland ecosystem models—can be determined. The present model does not directly fall into this class of systems: (1.1) contains three components and has a nonlinear diffusion term—unlike the systems considered in Carter et al. (2023). Nevertheless, we show in this paper that the methods by which the criteria in Carter et al. (2023) are deduced can also be applied to the present modified Gatenby-Gawlinski model.

As in Carter et al. (2023), the transversal (in)stability results are derived from a detailed investigation into the structure of the (one-dimensional) traveling front on which the evolving two-dimensional interface is based (see Fig. 1). These fronts correspond to heteroclinic connections between stable background states—or homogeneous equilibria—in (1.1). The background states of (1.1) are given by

$$
P_1 = (0, 0, 0), \quad P_2 = (1, 0, 0), \quad P_3^\pm = (1 - \delta_1 V^\pm, V^\pm, V^\pm), \quad P_4^\pm = (0, V^\pm, V^\pm), \tag{1.2}
$$
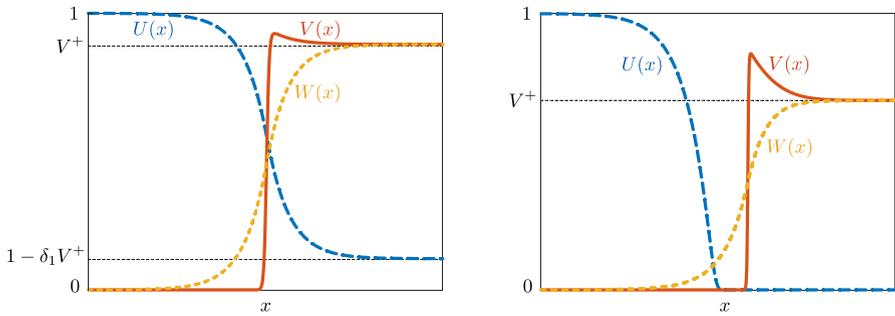
Fig. 2 Bistable traveling front solutions in the benign (left) and malignant (right) cases. Note that in the malignant case, an acellular gap may appear in between the interfaces formed by the U and V profiles and that this case corresponds to the situation of Fig. 1

with

$$V^{\pm} = \frac{\rho(1+a) - \delta_2 \pm \sqrt{(\rho(1+a) - \delta_2)^2 - 4\rho^2 a}}{2\rho}, \tag{1.3}$$

where we note that the states $P_3^{\pm}$ only are biologically relevant for parameter combinations such that $V^{\pm}$ are real and positive and $\delta_1 V^+ < 1$, and $P_4^{\pm}$ for parameters such that $V^{\pm} > 0$. It follows from linear stability analysis (see Appendix A) that P_2 is stable, while P_1, P_3^-, P_4^- are unstable. The background state P_3^+ is stable for $\delta_1 V^+ < 1$, while P_4^+ is stable if $\delta_1 V^+ > 1$. In this paper, we refer to the former as the *benign* case, and the latter as the *malignant* case, based on whether normal cells U can coexist with tumor cells V in the nontrivial stable steady state. In the benign case $\delta_1 V^+ < 1$ we will construct (and further study) a bistable traveling front between homogeneous background states P_2 and P_3^+, while in the malignant case $\delta_1 V^+ > 1$, we will consider a bistable front between P_2 and P_4^+—see Fig. 2.

We construct three types of bistable traveling fronts/tumor interfaces using geometric singular perturbation theory: a benign front, a malignant no-gap front and a malignant gap front (see upcoming Fig. 6 for the distinct geometries of these cases). The overall geometry of the construction of fronts is similar to that of Davis et al. (2022), in which invasion fronts were constructed in the model (1.1) in the absence of the Allee effect. Some differences arise here due to the presence of the Allee effect, which results in bistable fronts existing at a unique wave speed, as opposed to a range of speeds. These bistable fronts are more amenable to a two-dimensional stability analysis, as the critical spectrum associated with such fronts in one spatial dimension takes the form of a single eigenvalue at $\lambda = 0$ due to translation invariance. As in Carter et al. (2023), we do not explicitly analyze the longitudinal, i.e. one-dimensional (in the direction of propagation), stability of these traveling fronts: we assume that they are longitudinally stable and thus that the translational eigenvalue at $\lambda = 0$ is the most critical eigenvalue. Note that the assumptions are based on numerical observations and especially on numerical evaluations of the spectrum associated with the linearized stability problem (cf. Sect.4). The stability of the associated planar interface

spanned by the one-dimensional fronts can be determined by an additional transversal Fourier expansion—parameterized by wavenumber $\ell \in \mathbb{R}$. As a consequence, the translational eigenvalue re-appears as a local extremum at $\ell = 0$ of a critical curve $\lambda_c(\ell)$, i.e. $\lambda_c(0) = 0$. Observe that this curve is symmetric in ℓ. Extending the methods developed in Carter et al. (2023), we derive an explicit approximation of $\lambda_c''(0)$, where prime denotes differentiation with respect to ℓ. Clearly, the interface is unstable with respect to transversal long wavelength perturbations if $\lambda_c''(0) > 0$ (so that $\lambda_c(\ell) > 0$ for ℓ sufficiently small). In that case, the originally planar interface will be unstable and growing long wavelength spatial structures will emerge from the interface. Numerical simulations show that the interface may develop protruding fingers (Fig. 1) or cusps (see Sect. 4), which is similar to the observations of evolving interfaces (between grasslands and bare soil) in dryland ecosystems under the same circumstances (i.e. also with $\lambda_c''(0) > 0$) (Carter 2024; Carter et al. 2023; Fernandez-Oto et al. 2019).

The explicit character of our analysis establishes a direct correspondence between the nature—benign, malignant no-gap/gap—of the underlying traveling front and the initiation of transversal instabilities of the evolving interface between tumorous and regular cells. We briefly summarize some of our main findings (and refer to Sect. 4 for the more extensive discussion): Firstly, we deduce directly from our derivation of $\lambda_c''(0)$, and from the geometry of the associated front, that the presence of the acellular gap immediately implies transversal instability of the tumor interface in this model for sufficiently small $\varepsilon > 0$. In the benign and malignant no-gap cases, however, the tumor interface can be stable or unstable to long wavelength perturbations depending on parameters. Our characterization of this instability in terms of the coefficient $\lambda_c''(0)$ allows us to easily determine stability boundaries in parameter space via numerical continuation; see Sect. 4. We also explore the effect of individual parameters, such as the parameter δ_1, which turns out to be a natural parameter to transition between the three cases of benign and malignant no-gap/gap fronts, and the Allee parameter a. In particular, for the latter, we find that in general a stronger Allee effect, i.e. larger a, leads to a decrease in the speed of the associated front, but also leads to the onset of the transversal instability.

The remainder of the paper is organized as follows. In Sect. 2, we analyze the traveling wave equation associated with (1.1) to describe the existence construction of traveling fronts in the singular limit $\varepsilon \to 0$. Using formal singular perturbation arguments we examine the transversal long wavelength (in)stability of these fronts in Sect. 3, and we conclude with numerical simulations and a discussion in Sect. 4.

2 Existence of traveling fronts

In this section, we show that (1.1) supports traveling fronts. We will largely follow the geometric singular perturbation theory approach of Davis et al. (2022). In Davis et al. (2022) the formal asymptotic results of Holder et al. (2014) on the original nondimensionalized Gatenby-Gawlinski model were proven rigorously and a geometric interpretation of the benign and malignant cases, as well as the acellular gap, were given. As the focus of the current manuscript is largely on the stability of the traveling fronts, see Sect. 3, and since the derivation of the existence results for the

current setting largely mimics the approaches and proofs of Davis et al. (2022), we only succinctly derive the results (and we refer to Davis et al. (2022) for the rigorous constructions in a similar setting).

We set $(U, V, W)(x, y, \tau) = (u, v, w)(x + \varepsilon^\nu c\tau)$ and search for traveling waves in the traveling coordinate $\xi := x + \varepsilon^\nu c\tau$, where $c > 0$. This results in a singularly perturbed traveling wave ordinary differential equation (ODE)

$$
\begin{aligned}
\varepsilon^\nu cu' &= u(1 - u) - \delta_1 uw, \\
\varepsilon^\nu cv' &= \rho v(1 - v)(v - a) - \delta_2 vw + ((1 + \kappa - u)v')', \\
\varepsilon^\nu cw' &= \delta_3(v - w) + \frac{1}{\varepsilon^2}w'',
\end{aligned}
\tag{2.1}
$$

where $'$ means differentiation with respect to ξ. Upon introducing[1] $q := \varepsilon^{-\nu}(1 + \kappa - u)v' - cv$ and $p = w'/\varepsilon$, we rewrite this system as a first order slow/fast ODE

$$
\begin{aligned}
\varepsilon^\nu u' &= \frac{u}{c}(1 - u - \delta_1 w), \\
v' &= \varepsilon^\nu \frac{q + cv}{1 + \kappa - u}, \\
\varepsilon^\nu q' &= -\rho v(1 - v)(v - a) + \delta_2 vw, \\
w' &= \varepsilon p, \\
p' &= \varepsilon \left(c\varepsilon^{\nu+1} p - \delta_3(v - w) \right).
\end{aligned}
\tag{2.2}
$$

Observe that the v-equation of (2.2) is not singular due to the regularisation term κ and the fact that we are looking for traveling fronts with normal cell density u between 0 and 1. The fixed points

$$
\begin{aligned}
p_1 &= (0, 0, 0, 0, 0), \quad p_2 = (1, 0, 0, 0, 0), \\
p_3^\pm &= (1 - \delta_1 V^\pm, V^\pm, cV^\pm, V^\pm, 0), \quad p_4^\pm = (0, V^\pm, cV^\pm, V^\pm, 0),
\end{aligned}
$$

of (2.2) in (u, v, q, w, p)-space correspond to the steady states P_1, P_2, $P_3^\pm$, $P_4^\pm$ (1.2) of (1.1).

We observe three critical ν-cases in (2.2): $\nu = 0$ and $\nu = \pm 1$. In Holder et al. (2014) it was shown for the original nondimensionalized Gatenby-Gawlinski model that, when translated to the current setting, the case $\nu = 1$ does not lead to traveling fronts. In contrast, the case $\nu = -1$ led to *fast traveling fronts*, while the case $\nu = 0$ led to *slow traveling fronts*. In Davis et al. (2022) both the fast traveling fronts and slow traveling fronts were investigated. Based on our numerical simulations it appears that the $\nu = 0$-case is the most relevant for the instabilities we want to study. Therefore, we focus on the $\nu = 0$-case and only briefly highlight the $\nu = -1$-case in the remark below.

---

[1] See Remark 2.1 of Davis et al. (2022) for the rationale behind this non-standard scaling.
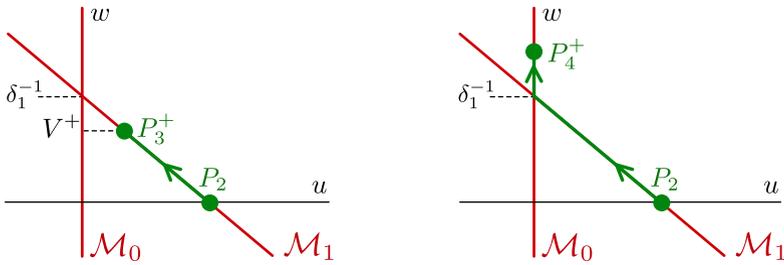
Fig. 3 Schematic of the singular heteroclinic orbit in the benign case where $u \neq 0$ after the invasion of the traveling wave (left) and the malignant case where $u = 0$ after the invasion (right)

For $v = 0$ in (2.2) we observe that (u, v, q) are *fast variables*, while (w, p) are *slow variables*. Letting $\varepsilon \to 0$, we find the critical manifolds

$$\mathcal{M}_0 = \{(u, v, q, w, p) \mid u = 0, \ q = -cv, \ \rho v(1 - v)(v - a) = \delta_2 v w\},$$
$$\mathcal{M}_1 = \{(u, v, q, w, p) \mid u = 1 - \delta_1 w, \ q = -cv, \ \rho v(1 - v)(v - a) = \delta_2 v w\},$$
$$(2.3)$$

which meet along the nonhyperbolic transcritical singularity curve at $w = 1/\delta_1$. The fixed points $p_1, p_4^\pm$ lie on $\mathcal{M}_0$, while $p_2, p_3^\pm$ lie on $\mathcal{M}_1$. In the benign case $\delta_1 V^+ < 1$, see (1.3), we can construct a singular heteroclinic orbit between p_2 and p_3^+ in the subspace $u = 1 - \delta_1 w$, that is, the orbit is entirely contained within $\mathcal{M}_1$ and avoids the transcritical singularity; see Fig. 3. In the malignant case $\delta_1 V^+ > 1$, we can construct a singular heteroclinic orbit between p_2 and p_4^+, but it necessarily passes through the transcritical curve in order to transition from $\mathcal{M}_1$ to $\mathcal{M}_0$.

In order to construct singular heteroclinic orbits in each case, we consider the associated layer problems describing the dynamics near the interface (the *fast field*) and reduced problems describing the dynamics away from the interface (the *slow fields*) in the next sections.

Remark 2.1 For the fast traveling fronts with $\nu = -1$, the singularly perturbed problem reduces, upon rescaling space once more, at leading order to

$$\dot{u} = \frac{u}{c}(1 - u - \delta_1 w),$$
$$\dot{q} = -\rho v(1 - v)(v - a) + \varepsilon^2 \delta_2 v w,$$
$$\dot{w} = p,$$
$$\dot{p} = cp - \delta_3(v - w),$$

where $\cdot$ denotes differentiation with respect to $\bar{\xi} := \varepsilon x + ct$, on the attracting four dimensional critical manifold

$$\mathcal{M}_0^F := \left\{(u, v, q, w, p) \ \middle| \ v = -\frac{q}{c}\right\}.$$

That is, the existence of fast traveling fronts boils down to showing the existence of heteroclinic solutions to

$$\dot{u} = \frac{u}{c}(1 - u - \delta_1 w) \,,$$
$$c\dot{v} = \rho v(1 - v)(v - a) - \delta_2 vw \,,$$
$$\ddot{w} - c\dot{w} = -\delta_3(v - w) \,.$$

In this manuscript, we do not pursue this direction any further; however, see Theorem 1.1 of Davis et al. (2022).

2.1 Layer problem

We consider the layer problem describing the dynamics near the interface (the fast field) for $v = 0$. That is, we set $v = 0$ in (2.2) and take the singular limit $\varepsilon \to 0$ to obtain

$$u' = \frac{u}{c}(1 - u - \delta_1 w) \,,$$
$$v' = \frac{q + cv}{1 + \kappa - u} \,, \tag{2.4}$$
$$q' = -\rho v(1 - v)(v - a) + \delta_2 vw \,,$$

where we recall that $'$ denotes differentiation with respect to $\xi = x + ct$, with the fast variables w and p fixed constants. The fixed points of (2.4) are related to the critical manifolds $\mathcal{M}_{0,1}$ (2.3), and note that these have several branches
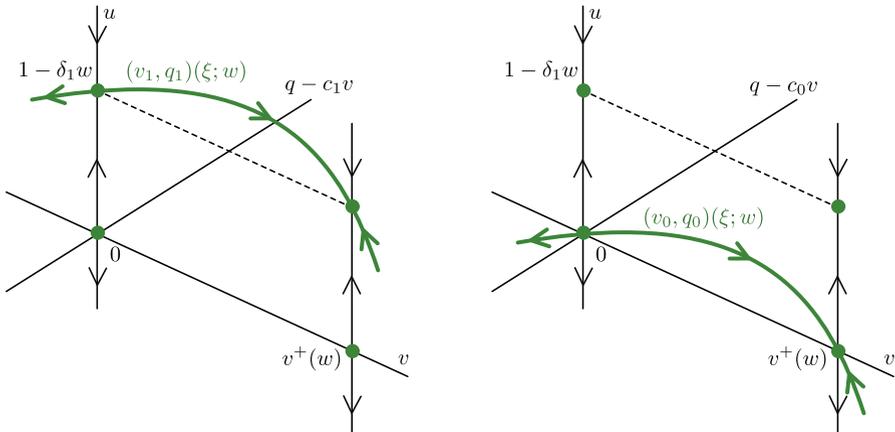
$$\mathcal{M}_0^0 = \{(u, v, q, w, p) \mid u = v = q = 0\} \,,$$
$$\mathcal{M}_0^\pm = \{(u, v, q, w, p) \mid u = 0, \ v = v^\pm(w), \ q = -cv^\pm(w)\} \,,$$
$$\mathcal{M}_1^0 = \{(u, v, q, w, p) \mid u = 1 - \delta_1 w, \ v = q = 0\} \,,$$
$$\mathcal{M}_1^\pm = \{(u, v, q, w, p) \mid u = 1 - \delta_1 w, \ v = v^\pm(w), \ q = -cv^\pm(w)\} \,,$$

where

$$v^\pm(w) = \frac{1 + a \pm \sqrt{(1 - a)^2 - 4\delta_2 w/\rho}}{2} \,.$$

We note that the fixed point p_2 lies on $\mathcal{M}_1^0$, while p_3^+ lies on $\mathcal{M}_1^+$, and p_4^+ lies on $\mathcal{M}_0^+$. By inspecting the Jacobian matrix of (2.4)

$$J = \begin{pmatrix} \frac{1}{c}(1 - 2u - \delta_1 w) & 0 & 0 \\ \frac{q+cv}{(1+\kappa-u)^2} & \frac{c}{1+\kappa-u} & \frac{1}{1+\kappa-u} \\ 0 & \rho(3v^2 - 2av + a) + \delta_2 w & 0 \end{pmatrix}$$

Fig. 4 (Left) The fast orbit $(v_1, q_1)(\xi; w)$ in the subspace $u = 1 - \delta_1 w$ with $0 \le w < \min\{\rho(1 - a)^2/(4\delta_2), 1/\delta_1\}$. (Right) The fast orbit $(v_0, q_0)(\xi; w)$ in the subspace $u = 0$ with $w > 0$

and noting the lower block triangular structure of this matrix, we see that the critical manifolds all lose normal hyperbolicity along the transcritical curve $w = \delta_1^{-1}$ where $1 - 2u - \delta_1 w = 0$ and along the fold curve where $v^+(w) = v^-(w)$, or equivalently $\rho(3v^2 - 2av + a) + \delta_2 w = 0$. Away from these curves, the manifolds $\mathcal{M}_0^0$, $\mathcal{M}_1^0$, $\mathcal{M}_0^+$, and $\mathcal{M}_1^+$ are all normally hyperbolic and of saddle type in the (v, q)-subsystem. The manifolds $\mathcal{M}_0^-$ and $\mathcal{M}_1^-$ are of center type when $c = 0$ and normally repelling/attracting in the (v, q)-subsystem when $c \lessgtr 0$; however these two manifolds will not be important for the analysis.

Importantly, for the benign case $u = 1 - \delta_1 w$ in the layer dynamics and for each $0 \le w < \min\{\rho(1 - a)^2/(4\delta_2), 1/\delta_1\}$ (within this subspace $u = 1 - \delta_1 w$) there exists a heteroclinic orbit $(v, q) = (v_1, q_1)(\xi; w)$ between $\mathcal{M}_1^0$ and $\mathcal{M}_1^+$ satisfying the planar ODE

$$v' = \frac{q + cv}{\kappa + \delta_1 w},$$
$$q' = -\rho v(1 - v)(v - a) + \delta_2 vw,$$

with $c = c_1(w)$, see Fig. 4. Here, $v_1(\xi; w)$ and $c_1(w)$ are given by

$$v_1(\xi; w) := \frac{v^+(w)}{2}\left(1 + \tanh\left(\frac{v^+(w)}{2}\sqrt{\frac{\rho}{2(\kappa + \delta_1 w)}}\xi\right)\right),$$

$$c_1(w) := \sqrt{\frac{2(\kappa + \delta_1 w)}{\rho}}\left(\frac{v^+(w)}{2} - v^-(w)\right).$$

Similarly, in the subspace $u = 0$, there exists a heteroclinic orbit $(v, q) = (v_0, q_0)(\xi; w)$ between $\mathcal{M}_0^0$ and $\mathcal{M}_0^+$ satisfying the planar ODE

$$v' = \frac{q + cv}{1 + \kappa},$$
$$q' = -\rho v(1 - v)(v - a) + \delta_2 vw,$$

for $c = c_0(w)$, where

$$v_0(\xi; w) := \frac{v^+(w)}{2} \left(1 + \tanh \left(\frac{v^+(w)}{2} \sqrt{\frac{\rho}{2(1 + \kappa)}} \xi \right) \right),$$

$$c_0(w) := \sqrt{\frac{2(1 + \kappa)}{\rho}} \left(\frac{v^+(w)}{2} - v^-(w) \right).$$

2.2 Reduced problem

Rescaling $\zeta = \varepsilon \xi$ and setting $\varepsilon = 0$, we obtain the reduced problem describing the dynamics away from the interface (the slow fields)

$$w_\zeta = p,$$
$$p_\zeta = -\delta_3(v - w),$$

which does not explicitly depend on u and describes the leading order dynamics on the critical manifolds. When restricted to $\mathcal{M}_0^0$ or $\mathcal{M}_1^0$, where $v = 0$, this results in the system

$$\begin{aligned} w_\zeta &= p, \\ p_\zeta &= \delta_3 w, \end{aligned} \tag{2.5}$$

while on $\mathcal{M}_0^+$ and $\mathcal{M}_1^+$, where $v = v^+(w)$, we have the system

$$\begin{aligned} w_\zeta &= p, \\ p_\zeta &= \delta_3(w - v^+(w)). \end{aligned} \tag{2.6}$$

The system (2.5) admits a saddle equilibrium at $(0, 0)$ corresponding to the fixed point p_2 of the full system, while (2.6) admits a saddle equilibrium at $(V^+, 0)$, see (1.3), corresponding to p_3^+ or p_4^+. The (un)stable manifolds $\mathcal{W}^{s,u}(0, 0)$ of the equilibrium $(0, 0)$ of (2.5) within $\mathcal{M}_0^0$ or $\mathcal{M}_1^0$ are given by the lines $\{p = \pm\sqrt{\delta_3}w\}$, while the (un)stable manifolds $\mathcal{W}^{s,u}(V^+, 0)$ of the equilibrium $(V^+, 0)$ of (2.6) within $\mathcal{M}_0^+$ or $\mathcal{M}_1^+$ can be determined (implicitly) from the Hamiltonian structure of (2.6). In particular, the quantities

$$E_0(w, p) := \frac{1}{2}p^2 - \frac{\delta_3}{2}w^2,$$
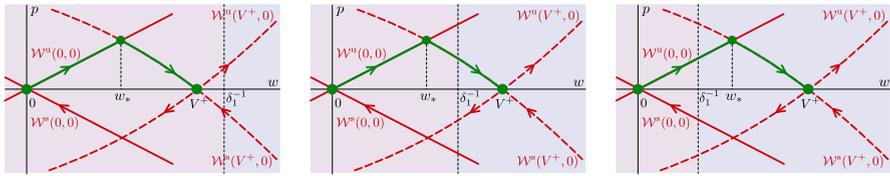
Fig. 5 The slow orbits on $\mathcal{M}_{0,1}^0$ and $\mathcal{M}_{0,1}^+$, corresponding to $\mathcal{W}^u(0,0)$ and $\mathcal{W}^u(V^+,0)$, respectively, in the benign (left), malignant no-gap (center), and malignant gap (right) cases. The manifolds $\mathcal{W}^{s,u}(0,0)$ on $\mathcal{M}_{0,1}^0$ are depicted in solid red, while the manifolds $\mathcal{W}^{s,u}(V^+,0)$ on $\mathcal{M}_{0,1}^+$ are depicted in dashed red, and the vertical dashed line indicates the subspace $w = \delta_1^{-1}$ at which the reduced dynamics transition from $\mathcal{M}_0^{0,+}$ to $\mathcal{M}_1^{0,+}$; see also Fig. 6

and

$$E_+(w, p) := E_0(w, p) + E(w) = \frac{1}{2}p^2 - \frac{\delta_3}{2}w^2 + \frac{\delta_3}{2}(V^+)^2 + \int_{V^+}^w \delta_3 v^+(s)\,ds\,,$$

are conserved in (2.5) and (2.6), respectively, and satisfy

$$E_0(0,0) = 0 = E_+(V^+, 0)\,.$$

The equations (2.5) and (2.6) only differ by the term $\delta_3 v^+(w)$ in p-component and this term is always strictly positive. Furthermore, the flow of (2.6) through the line segment $\{(w, p) = (0,0) + t(V^+, 0) \mid t \in (0,1)\}$ is downwards, while the flow through $\{(w, p) = (V^+, 0) + t(0, \sqrt{\delta_3}V^+) \mid t \in (0,1)\}$ points to the right. Hence the projection of the unstable manifold $\mathcal{W}^u(0,0)$ from $\mathcal{M}_1^0$ onto $\mathcal{M}_1^+$ transversely intersects the stable manifold $\mathcal{W}^s(V^+, 0)$ of the equilibrium $(V^+, 0)$ at some $(w, p) = (w_*, p_*)$, where $p_* = \sqrt{\delta_3}w_*$, and $0 < w_* < V^+$ satisfies

$$E_+(w_*, \sqrt{\delta_3}w_*) = 0\,,$$

or equivalently,

$$0 = (V^+)^2 + \int_{V^+}^{w_*} \left(1 + a + \sqrt{(1-a)^2 - \frac{4\delta_2 z}{\rho}}\right) dz\,, \tag{2.7}$$

see Fig. 5. The same holds regarding the projection of the unstable manifold $\mathcal{W}^u(0,0)$ from $\mathcal{M}_0^0$ onto $\mathcal{M}_0^+$, which transversely intersects the stable manifold $\mathcal{W}^s(W^+, 0)$ of the equilibrium $(W^+, 0)$ at $w = w_*$.

2.3 Singular heteroclinic orbits

Combining orbits from the reduced and layer problems, we can construct singular heteroclinic orbits in the benign ($\delta_1 V^+ < 1$) and malignant ($\delta_1 V^+ > 1$) cases.
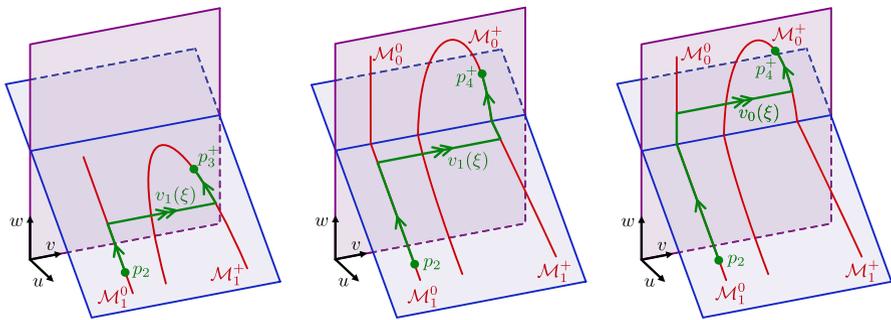
Fig. 6 Structure of the singular heteroclinic orbit in the benign (left), malignant no-gap (middle), and malignant gap (right) cases. The subspace $\{u = 0\}$ is depicted in purple, while the subspace $\{u = 1 - \delta_1 w\}$ is depicted in blue

Benign case: In the benign case, we construct a singular heteroclinic orbit between p_2 and p_3^+ by concatenating the three orbit segments, see Fig. 5 (left panel) and Fig. 6 (left panel):

1. slow orbit on $\mathcal{M}_1^0$ given by $\mathcal{W}^u(0, 0) \cap \{0 \leq w \leq w_*\}$, with $w^* < V^+$.
2. fast jump $(v_*, q_*)(\xi) := (v_1, q_1)(\xi; w_*)$ with speed $c = c_*(w) := c_1(w_*)$ in the layer problem (2.4) for $w = w_*$ in the subspace $u = 1 - \delta_1 w_*$, where w_* is defined as in (2.7), see Fig. 4. Note that $\delta_1 w_* < 1$ in the benign case.
3. slow orbit on $\mathcal{M}_1^+$ given by $\mathcal{W}^s(V^+, 0) \cap \{w_* < w \leq V^+\}$.

In the benign case, $\mathcal{M}_1^0$ and $\mathcal{M}_1^+$ are normally hyperbolic in the relevant region, and the fast jump is transversely constructed (with the speed $c \approx c_1(w_*)$ as a free parameter). Therefore, we expect that the singular orbit perturbs to a traveling front of the full problem for $0 < \varepsilon \ll 1$.

Malignant case: In the malignant case, we construct a heteroclinic orbit between p_2 and p_4^+, which necessarily crosses through the transcritical curve $w = \delta_1^{-1}$, see Fig. 3. However, we must split this into a further two cases, namely whether the corresponding value of w_* (as defined in (2.7)) satisfies $w_* \lessgtr \delta_1^{-1}$, as this determines whether the fast jump in the layer problem (2.4) occurs in the subspace $u = 0$ or $u = 1 - \delta_1 w$. That is, whether the fast jump occurs *before* of *after* crossing the transcritical curve. In the latter case $w_* > \delta_1^{-1}$, there is a region in which the values of both u, v are zero, *before* the fast jump occurs, that is, the front admits a gap, called the acellular gap, where only acid is present. In the former case $w_* < \delta_1^{-1}$ there is no acellular gap (as in the benign case above). The boundary between these cases in parameter space is determined by the condition

$$0 = (V^+)^2 + \int_{V^+}^{\delta_1^{-1}} 1 + a + \sqrt{(1 - a)^2 - \frac{4\delta_2 z}{\rho}} \, dz \,,$$

where V^+ is as in (1.3). We refer to these (sub)cases as the malignant gap and malignant no-gap cases, respectively.
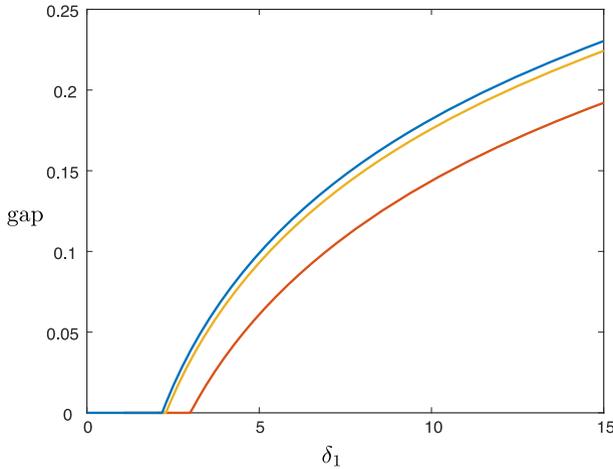
Fig. 7 Plot of gap width versus $\delta_1 \in (0.1, 15)$ obtained by numerical continuation of the traveling wave equation (2.2) for the parameter values $(a, \kappa, \delta_2, \delta_3, \rho) = (0.1, 0.1, 0.1, 70, 1.0)$ and $\varepsilon = 0.0063$ (red), $\varepsilon = 10^{-4}$ (yellow). The gap width was computed by measuring the spatial width where both the u and v profiles of the corresponding front solution were below a threshold value of 10ε. Also plotted (blue) is the singular limit gap width obtained by solving (2.7) for w_* using Mathematica and integrating (2.5) to obtain the time spent along $\mathcal{M}_0^0$ between $w = \delta_1^{-1}$ and $w = w_*$

In the **malignant no-gap case** $w_* < \delta_1^{-1}$, we have the following singular concatenation, see Fig. 5 (middle panel) and Fig. 6 (middle panel):

1. slow orbit on $\mathcal{M}_1^0$ given by $\mathcal{W}^u(0, 0) \cap \{0 \le w \le w_*\}$.
2. fast jump $(v_*, q_*)(\xi) := (v_1, q_1)(\xi; w_*)$ with speed $c = c_*(w) := c_1(w_*)$ in the layer problem (2.4) for $w = w_*$ in the subspace $u = 1 - \delta_1 w_*$, where w_* is defined as in (2.7), see Fig. 4. Note that $\delta_1 w_* < 1$ in the malignant no-gap case.
3. slow orbit on $\mathcal{M}_1^+$ given by $\mathcal{W}^s(V^+, 0) \cap \{w_* < w \le \delta_1^{-1}\}$.
4. slow orbit on $\mathcal{M}_0^+$ given by $\mathcal{W}^s(V^+, 0) \cap \{\delta_1^{-1} \le w < V^+\}$.

In the **malignant gap case** $w_* > \delta_1^{-1}$, we have the concatenation, see Fig. 5 (right panel) and Fig. 6 (right panel):

1. slow orbit on $\mathcal{M}_1^0$ given by $\mathcal{W}^u(0, 0) \cap \{0 \le w \le \delta_1^{-1}\}$.
2. slow orbit on $\mathcal{M}_0^0$ given by $\mathcal{W}^u(0, 0) \cap \{\delta_1^{-1} < w \le w_*\}$.
3. fast jump $(v_*, q_*)(\xi) := (v_0, q_0)(\xi; w_*)$ with speed $c = c_*(w) := c_0(w_*)$ in the layer problem (2.4) for $w = w_*$ in the subspace $u = 0$, where w_* is defined as in (2.7), see Fig. 4. Note that $\delta_1 w_* > 1$ in this case.
4. slow orbit on $\mathcal{M}_0^+$ given by $\mathcal{W}^s(V^+, 0) \cap \{w_* < w \le W^+\}$.

The acellular gap manifests as the slow orbit portion $\mathcal{W}^u(0, 0) \cap \{\delta_1^{-1} \le w \le w_*\}$ on $\mathcal{M}_0^0$. In general, one expects the gap size to thus increase with δ_1; see Fig. 7.

In both cases (malignant gap and malignant no-gap), the singular orbit traverses the transcritical curve $\delta_1 w = 1$ along a slow orbit. In the critical crossover case $w_* = \delta_1^{-1}$, the fast jump occurs precisely along the transcritical singularity curve. Due to the lack of hyperbolicity which occurs at the transcritical bifurcation, the persistence of orbits

in the malignant case for $0 < \varepsilon \ll 1$ is nontrivial, necessitating the use of blow-up desingularization methods (Krupa and Szmolyan 2001). Nevertheless we assume their persistence for sufficiently small $\varepsilon > 0$.

3 Stability of planar tumor interfaces

Given a traveling front $(u_h, v_h, w_h)(\xi)$ with speed $c_h = c_*(w_*) + \mathcal{O}(\varepsilon)$ constructed using the slow/fast structure as in the preceding section, we now consider its spectral stability in two space dimensions, focusing on the long wavelength (in)stability criterion as explored in Carter et al. (2023). Thus, like in Carter et al. (2023), we do not explicitly analyze the stability of the front $(u_h, v_h, w_h)(\xi)$ with respect to longitudinal perturbations, i.e. perturbations that only depend on ξ (or x). If the front is longitudinally stable—as is strongly suggested by our numerical results—then the upcoming stability criterion determines the (in)stability of the front to long wavelength perturbations in the y-direction, i.e. transverse to the direction of propagation. (We again refer to Carter et al. (2023) for a review of the literature on methods by which the longitudinal (in)stability of a singular traveling front as $(u_h, v_h, w_h)(\xi)$ can be established analytically.) We also refer ahead to Sect. 4 for numerical evidence (see Fig. 8) that the traveling fronts under consideration are 1D spectrally stable.

3.1 Long wavelength (in)stability

In a comoving frame, we rewrite (1.1) as

$$
\begin{aligned}
U_\tau &= F(U, W) - cU_\xi, \\
V_\tau &= G(U, V, W) + \nabla \cdot ((1 + \kappa - U)\nabla V) - cV_\xi, \\
W_\tau &= H(V, W) + \frac{1}{\varepsilon^2}\Delta W - cW_\xi,
\end{aligned}
\tag{3.1}
$$

where

$$
F(U, W) = U(1 - U) - \delta_1 UW, \tag{3.2}
$$
$$
G(U, V, W) = \rho V(1 - V)(V - a) - \delta_2 VW, \tag{3.3}
$$
$$
H(V, W) = \delta_3(V - W), \tag{3.4}
$$

and $(U, V, W) = (U, V, W)(\xi, y, \tau)$. Upon substituting the ansatz $(U, V, W) = (u_h, v_h, w_h)(\xi) + (\bar{u}, \bar{v}, \bar{w})(\xi)e^{i\ell y + \lambda\tau}$ and $c = c_h$, this results in the linear eigenvalue problem

$$
\begin{aligned}
\lambda u &= F_u u + F_w w - c_h u_\xi, \\
\lambda v &= G_v v + G_w w + (1 + k - u_h)v_{\xi\xi} - c_h v_\xi - uv_{h,\xi\xi} - u_\xi v_{h,\xi} \\
&\quad - u_{h,\xi} v_\xi - \ell^2(1 + k - u_h)v, \\
\lambda w &= H_v v + H_w w + \frac{1}{\varepsilon^2}w_{\xi\xi} - c_h w_\xi - \frac{\ell^2}{\varepsilon^2}w,
\end{aligned}
\tag{3.5}
$$

where we have dropped the bars for convenience and we denote $F_u(\xi) := \partial_u F(u_h(\xi), w_h(\xi))$, etc. We write (3.5) in the form

$$
\mathbb{L}(\xi) \begin{pmatrix} u \\ v \\ w \end{pmatrix} = \lambda \begin{pmatrix} u \\ v \\ w \end{pmatrix} + \ell^2 \begin{pmatrix} 0 \\ (1 + \kappa - u_h)v \\ \frac{1}{\varepsilon^2} w \end{pmatrix} , \tag{3.6}
$$

where

$$
\mathbb{L}(\xi) := \begin{pmatrix} -c_h \partial_\xi + F_u & 0 & F_w \\ -v_{h,\xi\xi} - v_{h,\xi}\partial_\xi & (1 + \kappa - u_h)\partial_{\xi\xi} - c_h\partial_\xi + G_v - u_{h,\xi}\partial_\xi & G_w \\ 0 & H_v & \frac{1}{\varepsilon^2}\partial_{\xi\xi} - c_h\partial_\xi + H_w \end{pmatrix} .
$$

Due to translation invariance, the derivative $(u, v, w)(\xi) = (u_h, v_h, w_h)'(\xi)$ of the wave with respect to ξ satisfies (3.6) when $\lambda = \ell = 0$. To examine long-wavelength interfacial instabilities in the direction transverse to the front propagation, we expand about this solution for small $|\ell| \ll 1$, and noting the symmetry $\ell \to -\ell$ we obtain

$$
\lambda_c(\ell) = \lambda_{c,2}\ell^2 + \mathcal{O}(\ell^4) , \qquad \begin{pmatrix} u(\xi; \ell^2) \\ v(\xi; \ell^2) \\ w(\xi; \ell^2) \end{pmatrix} = \begin{pmatrix} u_{h,\xi}(\xi) \\ v_{h,\xi}(\xi) \\ w_{h,\xi}(\xi) \end{pmatrix} + \begin{pmatrix} \tilde{u}(\xi) \\ \tilde{v}(\xi) \\ \tilde{w}(\xi) \end{pmatrix} \ell^2 + \mathcal{O}(\ell^4) ,
$$

and substitute into (3.6) to obtain

$$
\mathbb{L} \begin{pmatrix} \tilde{u}(\xi) \\ \tilde{v}(\xi) \\ \tilde{w}(\xi) \end{pmatrix} = \lambda_{c,2} \begin{pmatrix} u_{h,\xi}(\xi) \\ v_{h,\xi}(\xi) \\ w_{h,\xi}(\xi) \end{pmatrix} + \begin{pmatrix} 0 \\ (1 + \kappa - u_h)v_{h,\xi}(\xi) \\ \frac{1}{\varepsilon^2} w_{h,\xi}(\xi) \end{pmatrix} .
$$

This results in the Fredholm solvability condition

$$
0 = \left\langle \lambda_{c,2} \begin{pmatrix} u_{h,\xi}(\xi) \\ v_{h,\xi}(\xi) \\ w_{h,\xi}(\xi) \end{pmatrix} + \begin{pmatrix} 0 \\ (1 + \kappa - u_h)v_{h,\xi}(\xi) \\ \frac{1}{\varepsilon^2} w_{h,\xi}(\xi) \end{pmatrix}, \begin{pmatrix} u^A(\xi) \\ v^A(\xi) \\ w^A(\xi) \end{pmatrix} \right\rangle_{L^2} , \tag{3.7}
$$

where $(u^A, v^A, w^A)(\xi)$ denotes the unique bounded solution to the adjoint equation

$$
\mathbb{L}^A(\xi) \begin{pmatrix} u(\xi) \\ v(\xi) \\ w(\xi) \end{pmatrix} = 0 , \tag{3.8}
$$

where the adjoint operator $\mathbb{L}^A$ is given by

$$
\mathbb{L}^A(\xi) = \begin{pmatrix} c_h\partial_\xi + F_u & v_{h,\xi}\partial_\xi & 0 \\ 0 & (1 + \kappa - u_h)\partial_{\xi\xi} + c_h\partial_\xi + G_v - u_{h,\xi}\partial_\xi & H_v \\ F_w & G_w & \frac{1}{\varepsilon^2}\partial_{\xi\xi} + c_h\partial_\xi + H_w \end{pmatrix} .
$$

Solving (3.7) for $\lambda_{c,2}$, we find

$$
\lambda_{c,2} = -\frac{\displaystyle\int_{\mathbb{R}} (1 + \kappa - u_{\mathrm{h}}(\xi))\, v_{\mathrm{h},\xi}(\xi) v^A(\xi) + \frac{1}{\varepsilon^2} w_{\mathrm{h},\xi}(\xi) w^A(\xi)\, \mathrm{d}\xi}{\displaystyle\int_{\mathbb{R}} u_{\mathrm{h},\xi}(\xi) u^A(\xi) + v_{\mathrm{h},\xi}(\xi) v^A(\xi) + w_{\mathrm{h},\xi}(\xi) w^A(\xi)\, \mathrm{d}\xi}.
\tag{3.9}
$$

We note that the sign of $\lambda_{c,2}$ determines the stability of the interface to transverse long wavelength perturbations. To estimate the expression (3.9), we need to obtain leading-order approximations of the adjoint solution $(u^A, v^A, w^A)(\xi)$.

3.2 Leading order asymptotics of $\lambda_{c,2}$

We consider the fast formulation

$$
\begin{aligned}
&c_{\mathrm{h}} u_\xi + F_u(u_{\mathrm{h}}(\xi), w_{\mathrm{h}}(\xi)) u + v_{\mathrm{h},\xi} v_\xi = 0, \\
&(1 + \kappa - u_{\mathrm{h}}) v_{\xi\xi} + c_{\mathrm{h}} v_\xi + G_v(u_{\mathrm{h}}(\xi), v_{\mathrm{h}}(\xi), w_{\mathrm{h}}(\xi)) v \\
&\quad + H_v(v_{\mathrm{h}}(\xi), w_{\mathrm{h}}(\xi)) w - u_{\mathrm{h},\xi} v_\xi = 0, \\
&w_{\xi\xi} + \varepsilon^2 c_{\mathrm{h}} w_\xi + \varepsilon^2 \big(F_w(u_{\mathrm{h}}(\xi), w_{\mathrm{h}}(\xi)) u + G_w(u_{\mathrm{h}}(\xi), v_{\mathrm{h}}(\xi), w_{\mathrm{h}}(\xi)) v \\
&\quad + H_w(v_{\mathrm{h}}(\xi), w_{\mathrm{h}}(\xi)) w \big) = 0,
\end{aligned}
\tag{3.10}
$$

of the adjoint equation (3.8), and the associated slow formulation

$$
\begin{aligned}
&\varepsilon c_{\mathrm{h}} u_\zeta + F_u(u_{\mathrm{h}}(\zeta/\varepsilon), w_{\mathrm{h}}(\zeta/\varepsilon)) u + \varepsilon^2 v_{\mathrm{h},\zeta} v_\zeta = 0, \\
&\varepsilon^2 (1 + \kappa - u_{\mathrm{h}}) v_{\zeta\zeta} + \varepsilon c_{\mathrm{h}} v_\zeta + G_v(u_{\mathrm{h}}(\zeta/\varepsilon), v_{\mathrm{h}}(\zeta/\varepsilon), w_{\mathrm{h}}(\zeta/\varepsilon)) v \\
&\quad + H_v(v_{\mathrm{h}}(\zeta/\varepsilon), w_{\mathrm{h}}(\zeta/\varepsilon)) w - \varepsilon^2 u_{\mathrm{h},\zeta} v_\zeta = 0, \\
&w_{\zeta\zeta} + \varepsilon c_{\mathrm{h}} w_\zeta + F_w(u_{\mathrm{h}}(\zeta/\varepsilon), w_{\mathrm{h}}(\zeta/\varepsilon)) u + G_w(u_{\mathrm{h}}(\zeta/\varepsilon), v_{\mathrm{h}}(\zeta/\varepsilon), w_{\mathrm{h}}(\zeta/\varepsilon)) v \\
&\quad + H_w(v_{\mathrm{h}}(\zeta/\varepsilon), w_{\mathrm{h}}(\zeta/\varepsilon)) w = 0,
\end{aligned}
\tag{3.11}
$$

where $\zeta = \varepsilon \xi$, and we abuse notation by writing $u = u(\xi)$ in (3.10), and $u = u(\zeta)$ in (3.11), etc. In the fast field near the interface, to leading order we have $c_{\mathrm{h}} = c_*(w_*)$, $w_{\mathrm{h}} = w_*$, $v_{\mathrm{h}} = v_*(\xi)$, and $u_{\mathrm{h}} = u_*$, where

$$
c_*(w_*) = \begin{cases} c_1(w_*), & w_* < \delta_1^{-1}, \\ c_0(w_*), & w_* > \delta_1^{-1}, \end{cases}
$$

$$
(v_*, q_*)(\xi; w_*) = \begin{cases} (v_1, q_1)(\xi; w_*), & w_* < \delta_1^{-1}, \\ (v_0, q_0)(\xi; w_*), & w_* > \delta_1^{-1}, \end{cases}
$$

$$
u_*(w_*) = \begin{cases} 1 - \delta_1 w_*, & w_* < \delta_1^{-1}, \\ 0, & w_* > \delta_1^{-1}. \end{cases}
$$

Thus, to leading order (3.10) becomes

$$c_* u_\xi + F_u(u_*, w_*)u + v_{*,\xi} v_\xi = 0,$$
$$(1 + \kappa - u_*)v_{\xi\xi} + c_* v_\xi + G_v(u_*, v_*(\xi), w_*)v + H_v(v_*(\xi), w_*)w = 0,$$
$$w_{\xi\xi} = 0.$$

Hence w is constant to leading order with $w = \bar{w}_*$, and v satisfies

$$(1 + \kappa - u_*)v_{\xi\xi} + c_* v_\xi + G_v(u_*, v_*(\xi), w_*)v = -H_v(v_*(\xi), w_*)\bar{w}_*. \qquad (3.12)$$

We define the fast reduced operator

$$\mathcal{L}_v := (1 + \kappa - u_*)\partial_{\xi\xi} - c_*\partial_\xi + G_v(u_*, v_*(\xi), w_*).$$

The unique bounded solution of the fast reduced adjoint equation

$$\mathcal{L}_v^A v = (1 + \kappa - u_*)v_{\xi\xi} + c_* v_\xi + G_v(u_*, v_*(\xi), w_*)v = 0$$

is given by $\bar{v}_*(\xi) := v_{*,\xi}(\xi)e^{-c_*\xi/(1+\kappa-u_*)}$.

Since $v_{*,\xi}$ lies in the kernel of $\mathcal{L}_v$, (3.12) implies that

$$0 = \bar{w}_* \int_\mathbb{R} H_v(v_*(\xi), w_*)v_{*,\xi}(\xi)d\xi = \bar{w}_* \left(H(v_*^+, w_*) - H(0, w_*)\right) = \delta_3 \bar{w}_* v_*^+,$$

where $v_*^+ := v^+(w_*) = \lim_{\xi\to\infty} v_*(\xi)$ and we recall that $\lim_{\xi\to-\infty} v_*(\xi) = 0$. Hence to leading order $\bar{w}_* = 0$ and $v(\xi) = \alpha_* \bar{v}_*(\xi)$. From this we see that u satisfies

$$c_* u_\xi + F_u(u_*, w_*)u + \alpha_* v_{*,\xi} \bar{v}_{*,\xi}(\xi) = 0$$

to leading order. Since $F_u(u_*, w_*) = 1 - 2u_* - \delta_1 w_* < 0$ (both for $\delta_1 w_* \lessgtr 1$) and since $u(\xi)$ must be bounded, it follows that

$$u(\xi) = \alpha_* \bar{u}_*(\xi) := -\frac{\alpha_*}{c_*} \int_\infty^\xi e^{-\frac{1}{c_*}(1-2u_*-\delta_1 w_*)(\xi-s)} v_{*,s}(s)\bar{v}_{*,s}(s)ds.$$

In the slow fields away from the interface, to leading order

$$(u_h(\zeta/\varepsilon), v_h(\zeta/\varepsilon), w_h(\zeta/\varepsilon)) = \left(u_*(w^\pm(\zeta)), f^\pm(w^\pm(\zeta)), w^\pm(\zeta)\right), \qquad (3.13)$$

where $w^-(\zeta)$ denotes the slow orbit of (2.5) on $\mathcal{M}_0^0 \cup \mathcal{M}_1^0$ corresponding to $\mathcal{W}^u(0, 0)$ and satisfies $w^-(0) = w_*$, and similarly $w^+(\zeta)$ denotes the slow orbit of (2.6) on $\mathcal{M}_0^+ \cup \mathcal{M}_1^+$ corresponding to $\mathcal{W}^s(W^+, 0)$ and satisfies $w^+(0) = w_*$. Note that whether w^- is contained entirely within $\mathcal{M}_1^0$, or whether w^+ is contained entirely within $\mathcal{M}_1^+$, depends on which case we are in, namely, the benign, malignant gap or no-gap cases.

To simplify the following computations, we use the analogous notation $f^{\pm}(w)$ to define the corresponding v coordinate along the slow orbits by

$$f^{-}(w) := 0, \qquad f^{+}(w) := v^{+}(w),$$

and we recall that

$$u_{*}(w) = \begin{cases} 1 - \delta_1 w, & w < \delta_1^{-1} \\ 0, & w > \delta_1^{-1}. \end{cases}$$

In the slow fields, the orbits $w^{\pm}$ therefore satisfy the existence problem

$$w_{\zeta\zeta}^{\pm} + H(f^{\pm}(w^{\pm}), w^{\pm}) = 0. \tag{3.14}$$

Thus, to leading order (3.11) becomes

$$F_u(u_*(w^{\pm}), w^{\pm})u = 0,$$
$$G_v(u_*(w^{\pm}), f^{\pm}(w^{\pm}), w^{\pm})v + H_v(f^{\pm}(w^{\pm}), w^{\pm})w = 0,$$
$$w_{\zeta\zeta} + F_w(u_*(w^{\pm}), w^{\pm})u + G_w(u_*(w^{\pm}), f^{\pm}(w^{\pm}), w^{\pm})v + H_w(f^{\pm}(w^{\pm}), w^{\pm})w = 0,$$

from which we deduce that $u = 0$, and

$$v = -\frac{H_v(f^{\pm}(w^{\pm}), w^{\pm})}{G_v(u_*(w^{\pm}), f^{\pm}(w^{\pm}), w^{\pm})} w,$$

so that w satisfies

$$w_{\zeta\zeta} + \left(H_w(f^{\pm}(w^{\pm}), w^{\pm}) - \frac{H_v(f^{\pm}(w^{\pm}), w^{\pm})}{G_v(u_*(w^{\pm}), f^{\pm}(w^{\pm}), w^{\pm})} G_w(u_*(w^{\pm}), f^{\pm}(w^{\pm}), w^{\pm}) \right) w = 0. \tag{3.15}$$

Noting that

$$(f^{\pm})'(w^{\pm}) = -\frac{G_w(u_*(w^{\pm}), f^{\pm}(w^{\pm}), w^{\pm})}{G_v(u_*(w^{\pm}), f^{\pm}(w^{\pm}), w^{\pm})},$$

the equation (3.15) becomes

$$w_{\zeta\zeta} + \left(H_w(f^{\pm}(w^{\pm}), w^{\pm}) + H_v(f^{\pm}(w^{\pm}), w^{\pm})(f^{\pm})'(w^{\pm}) \right) w = 0,$$

from which we deduce upon differentiating (3.14) that $w(\zeta) = \alpha^{\pm} w_{\zeta}^{\pm}(\zeta)$ in the slow fields.

We recall that in the fast field $\bar{w}_* = 0$ to leading order so that $w = \mathcal{O}(\varepsilon)$, and hence in the slow fields we take $w = \varepsilon \bar{\alpha}^{\pm} w_{\zeta}^{\pm} = \bar{\alpha}^{\pm} w_{\xi}^{\pm}$. Since $w_{\zeta}^{+}(0) = w_{\zeta}^{-}(0) = p_*$, to

ensure continuity, we take $\bar{\alpha}^+ = \bar{\alpha}^- = \bar{\alpha}$, so that $\bar{w}_* = \varepsilon \bar{\alpha} p_*$. The jump in w_ξ in the slow fields

$$
\begin{aligned}
\Delta_s w_\xi &= \lim_{\zeta \downarrow 0} w_\xi - \lim_{\zeta \uparrow 0} w_\xi = \bar{\alpha} \left[\lim_{\zeta \downarrow 0} w_{\xi\xi}^+ - \lim_{\zeta \uparrow 0} w_{\xi\xi}^- \right] = \varepsilon^2 \bar{\alpha} \left[\lim_{\zeta \downarrow 0} w_{\zeta\zeta}^+ - \lim_{\zeta \uparrow 0} w_{\zeta\zeta}^- \right] \\
&= -\varepsilon^2 \bar{\alpha} \left[H(v_*^+, w_*) - H(0, w_*) \right] = -\varepsilon^2 \bar{\alpha} \delta_3 v_*^+
\end{aligned}
$$

must be accounted for by the change over the fast field

$$
\Delta_f w_\xi = -\varepsilon^2 \alpha_* \int_{\mathbb{R}} F_w(u_*, w_*) \bar{u}_*(\xi) + G_w(u_*, v_*(\xi), w_*) \bar{v}_*(\xi) \mathrm{d}\xi \,,
$$

from which we obtain

$$
\frac{\bar{\alpha}}{\alpha_*} = \frac{\int_{\mathbb{R}} F_w(u_*, w_*) \bar{u}_*(\xi) + G_w(u_*, v_*(\xi), w_*) \bar{v}_*(\xi) \mathrm{d}\xi}{\delta_3 v_*^+}. \tag{3.16}
$$

We can now estimate (3.9). At leading order

$$
\begin{aligned}
\int_{\mathbb{R}} w_{h,\xi}(\xi) w^A(\xi) \mathrm{d}\xi &= \left(\int_{-\infty}^{-\frac{1}{\sqrt{\varepsilon}}} + \int_{-\frac{1}{\sqrt{\varepsilon}}}^{\frac{1}{\sqrt{\varepsilon}}} + \int_{\frac{1}{\sqrt{\varepsilon}}}^{\infty} \right) w_{h,\xi}^*(\xi) w^A(\xi) \mathrm{d}\xi \\
&= \bar{\alpha} \int_{-\infty}^{-\frac{1}{\sqrt{\varepsilon}}} (w_\xi^-)^2 \mathrm{d}\xi + \varepsilon^2 \bar{\alpha} \int_{-\frac{1}{\sqrt{\varepsilon}}}^{\frac{1}{\sqrt{\varepsilon}}} (q_*)^2 \mathrm{d}\xi + \bar{\alpha} \int_{\frac{1}{\sqrt{\varepsilon}}}^{\infty} (w_\xi^+)^2 \mathrm{d}\xi \\
&= \varepsilon \bar{\alpha} \left(\int_{-\infty}^{0} (w_\zeta^-)^2 \mathrm{d}\zeta + \int_{0}^{\infty} (w_\zeta^+)^2 \mathrm{d}\zeta \right) + \mathcal{O}(\varepsilon\sqrt{\varepsilon}) \,,
\end{aligned}
$$

and

$$
\int_{\mathbb{R}} v_{h,\xi}(\xi) v^A(\xi) \mathrm{d}\xi = \alpha_* \int_{\mathbb{R}} v_{*,\xi}(\xi)^2 e^{-c_* \xi/(1+\kappa - u_*)} \mathrm{d}\xi + \mathcal{O}(\varepsilon).
$$

We note that $u_{h,\xi} = \mathcal{O}(\varepsilon)$ in the fast field while $u^A(\xi) = 0$ to leading order in the slow fields, so by (3.9) and (3.16), we have that

$$
\begin{aligned}
\lambda_{c,2} &\sim -\frac{\bar{\alpha}}{\varepsilon \alpha_*} \frac{\left(\int_{-\infty}^{0} (w_\zeta^-)^2 \mathrm{d}\zeta + \int_{0}^{\infty} (w_\zeta^+)^2 \mathrm{d}\zeta \right)}{\int_{\mathbb{R}} v_{*,\xi}(\xi)^2 e^{-\left(\frac{c_*}{1+\kappa - u_*} \right)\xi} \mathrm{d}\xi} \\
&= -\frac{1}{\varepsilon \delta_3 v_*^+} \int_{\mathbb{R}} F_w(u_*, w_*) \bar{u}_*(\xi) + G_w(u_*, v_*(\xi), w_*) \bar{v}_*(\xi) \mathrm{d}\xi \\
&\quad \times \frac{\left(\int_{-\infty}^{0} (w_\zeta^-)^2 \mathrm{d}\zeta + \int_{0}^{\infty} (w_\zeta^+)^2 \mathrm{d}\zeta \right)}{\int_{\mathbb{R}} v_{*,\xi}(\xi)^2 e^{-\left(\frac{c_*}{1+\kappa - u_*} \right)\xi} \mathrm{d}\xi}
\end{aligned}
$$

$$= \frac{1}{\varepsilon \delta_3 v_*^+} \frac{\left(\int_{-\infty}^0 (w_\zeta^-)^2 \mathrm{d}\zeta + \int_0^\infty (w_\zeta^+)^2 \mathrm{d}\zeta \right)}{\int_{\mathbb{R}} v_{*,\xi}(\xi)^2 e^{-\left(\frac{c_*}{1+\kappa-u_*}\right)\xi} \mathrm{d}\xi} \left(\int_{\mathbb{R}} \delta_1 u_* \bar{u}_*(\xi) + \delta_2 v_*(\xi) \bar{v}_*(\xi) \mathrm{d}\xi \right)$$

(3.17)

at leading order in ε, where

$$\bar{v}_*(\xi) = v_{*,\xi}(\xi) e^{-\frac{c_*}{1+\kappa-u_*}\xi}$$

$$\bar{u}_*(\xi) = \frac{1}{c_*} \int_\xi^\infty e^{-\frac{1}{c_*}(1-2u_*-\delta_1 w_*)(\xi-s)} v_{*,s}(s) \bar{v}_{*,s}(s) \mathrm{d}s.$$

In particular, the sign of $\lambda_{c,2}$ is determined at leading order by

$$\mathrm{sign}\,(\lambda_{c,2}) = \mathrm{sign}\left(\int_{\mathbb{R}} \delta_1 u_* \bar{u}_*(\xi) + \delta_2 v_*(\xi) \bar{v}_*(\xi) \mathrm{d}\xi \right).$$

(3.18)

In the gap case, $u_* = 0$, so that $\lambda_{c,2}$ is always positive, provided $\delta_2 > 0$. However, in the no-gap case, $u_* = 1 - \delta_1 w_*$, so that

$$\int_{\mathbb{R}} \delta_1 u_* \bar{u}_*(\xi) + \delta_2 v_*(\xi) \bar{v}_*(\xi) \mathrm{d}\xi$$

$$= \int_{\mathbb{R}} \left[\frac{\delta_1 (1 - \delta_1 w_*)}{c_*} \int_\xi^\infty e^{-\frac{1}{c_*}(-1+\delta_1 w_*)(\xi-s)} v_{*,s}(s) \bar{v}_{*,s}(s) \mathrm{d}s \right.$$

$$\left. + \delta_2 v_*(\xi) v_{*,\xi}(\xi) e^{-\frac{c_*}{\kappa+\delta_1 w_*}\xi} \right] \mathrm{d}\xi.$$

This term could be positive or negative depending on the relation between δ_1, δ_2, and the other system parameters ρ, a, k, δ_3.

4 Numerical simulations and discussion

The formal geometric singular perturbation analysis of the preceding sections provides a framework by which we can understand the structure of 1D bistable traveling tumor fronts in (1.1), and in particular uncovers geometric mechanisms which distinguish between qualitatively different cases: benign and malignant no-gap/gap tumors. Furthermore, when extending a 1D profile as a straight planar interface in two spatial dimensions, the expression (3.17) provides a stability criterion for long wavelength perturbations in the direction along the interface, assuming that the corresponding traveling wave is stable in one spatial dimension.

While we can deduce from this expression and the arguments in Sect. 3.2 that, for instance, tumor interfaces in the malignant gap case are always unstable in two spatial dimensions when ε is sufficiently small, in other regimes the sign of the integral expression (3.18) is less apparent due to its implicit dependence on various system

parameters. However, we are able to explore different parameter regimes by numerically solving the traveling wave equation (2.1). Figure 8 depicts numerically computed traveling waves profiles for four different sets of parameters. The 1D spectra of the solutions are also shown, implying that these waves are stable in the longitudinal direction, so that when restricted to a one-dimensional domain, small perturbations of the wave decay in time. Also plotted is a continuation of the eigenvalue $\lambda_{c,2}(\ell)$ for small values of the wave number ℓ in each case, indicating they are all unstable in two spatial dimensions; we note that each profile exhibits an acellular gap, and hence this matches our theoretical prediction that such solutions are unstable in two dimensions.

Using the expression (3.9), we are also able to track this instability as a function of system parameters. Figure 9 depicts the results of numerical continuation in the parameter δ_1 (the other parameters are the same as the wave in the first row of Fig. 8). Note that while the waves can be 2D stable for smaller values of δ_1, for larger δ_1 the instability appears, matching the prediction of the asymptotic expression (3.17) that the interfaces are unstable in the malignant gap case—the gap appears as δ_1 increases; see Fig. 7. We also note that the speed of the front also increases in δ_1. In Fig. 10, we track the impact of the Allee effect on the coefficient $\lambda_{c,2}$. We see that in general, an increase in the Allee effect decreases the speed of the tumor, but also leads to the onset of the long wavelength instability.

By solving numerically for zeros of the expression (3.9), we can also track the stability boundary in parameter space. Figure 11 depicts the stability boundary in (δ_1, δ_2)-space for two different values of ε. Also shown is the curve which forms the boundary in parameter space between the benign and malignant tumors, which shows that both benign/malignant tumors can be stable/unstable and that in general, the interfaces are more likely to be unstable for larger values of δ_1, δ_2.

We emphasize that our analysis concerns spectral stability of the traveling fronts, and while these spectral computations may indicate instability, it is not easy to predict the resulting nonlinear behavior of the interface. Nevertheless, direct numerical simulations suggest that planar interfaces are in fact nonlinearly unstable, and the dynamics may lead to complex patterns at the tumor interface. Figure 12 depicts the results of direct numerical simulations for three different choices of the parameters (a, ε), initialized with 1D-stable traveling wave profiles taken from rows two through four of Fig. 8. Different manifestations of the long wavelength instability appear in each case: in the first simulation the interface develops cusps which remain bounded as the propagation speed of the advancing interface appears to increase, while in the second, the interface breaks up into growing finger patterns; the parameter values for these two simulations were taken from Gatenby and Gawlinski (1996) (with the exception of (a, δ_2, κ), which were not present in Gatenby and Gawlinski (1996)). The third and final simulation exhibits more elaborate growing finger patterns, which develop on a faster timescale. Note that the time taken for the instability to develop varies based on the magnitude of the coefficient $\lambda_{c,2}$; see Fig. 8.

From the mathematical point of view, there are a number of further research directions that are directly in line with the present work. More general models also include tumor cell density V in the nonlinear diffusion term of the evolution equation for V (1.1) and may also contain (nonlinear) diffusion on the U-equation. The methods developed here are believed to be sufficiently flexible to investigate more general
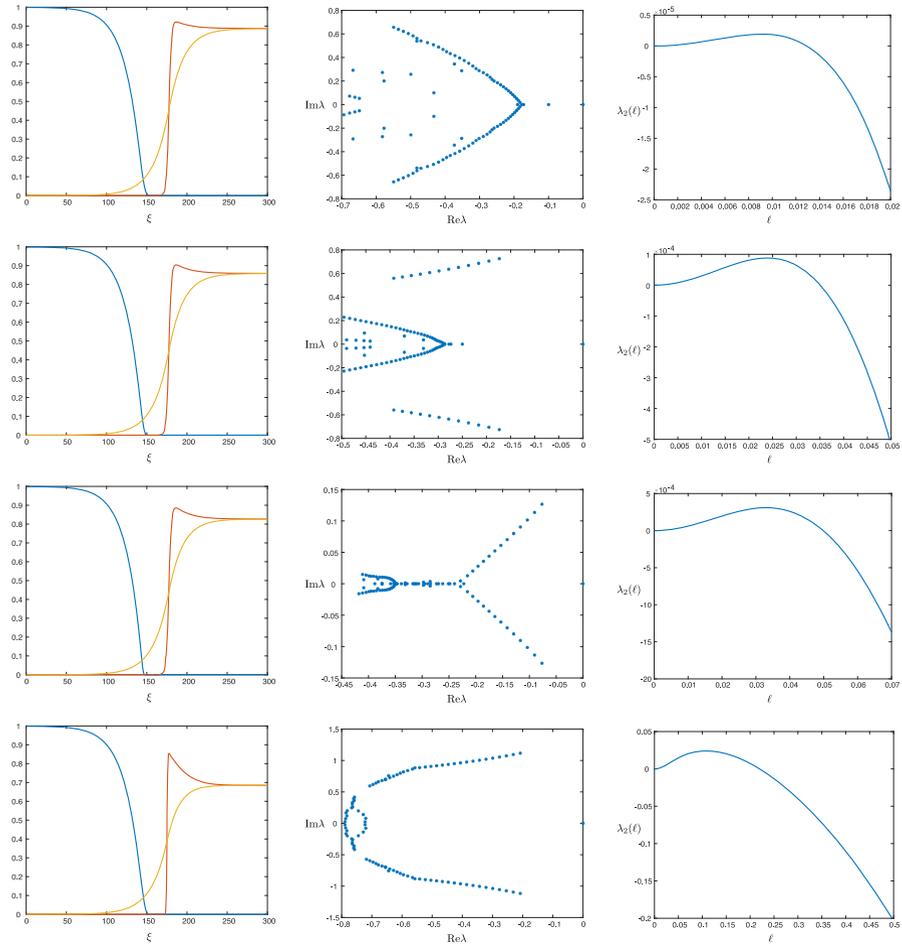
Fig. 8 1D traveling wave profiles obtained for the parameter values $(a, \kappa, \delta_1, \delta_2, \delta_3, \rho, \varepsilon) = (0.1, 0.1, 12.5, 0.1, 70, 1, 0.0063)$ (first row), $(a, \kappa, \delta_1, \delta_2, \delta_3, \rho, \varepsilon) = (0.25, 0.1, 12.5, 0.1, 70, 1, 0.0063)$ (second row), and $(a, \kappa, \delta_1, \delta_2, \delta_3, \rho, \varepsilon) = (0.35, 0.1, 12.5, 0.1, 70, 1, 0.0063)$ (third row), $(a, \kappa, \delta_1, \delta_2, \delta_3, \rho, \varepsilon) = (0.25, 0.05, 11.5, 3, 1, 15, 0.05)$ (fourth row). The u, v, w profiles are plotted in blue, red, yellow, respectively. Profiles were obtained by solving the traveling wave equation (2.1) in MATLAB. Also shown are the 1D spectra, providing numerical evidence that all four solutions are 1D-stable, as well as a continuation of the critical eigenvalue $\lambda_c(\ell)$ for small, positive values of the wavenumber ℓ

equations. Within the current framework, several open questions remain. In particular, the basic assumption underlying the two-dimensional stability analysis here (that is numerically validated in several cases, see Fig. 8) is the stability of the front with respect to one-dimensional (longitudinal) perturbations—a rigorous verification of this assumption is the subject of future work. In addition, our (in)stability results are purely at the spectral level, and a challenging direction for future work concerns the study of the nonlinear manifestation of the long wavelength instability studied here.
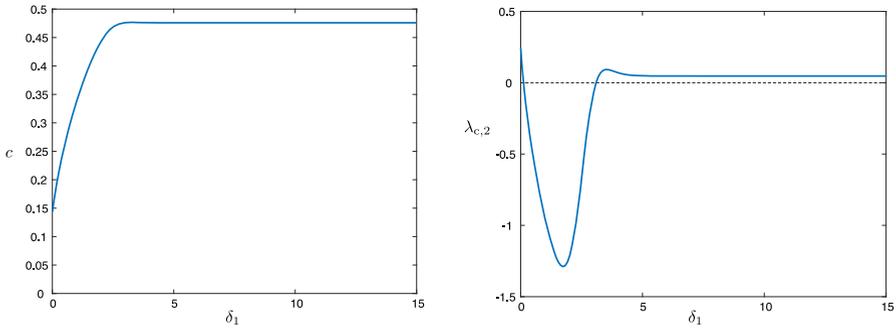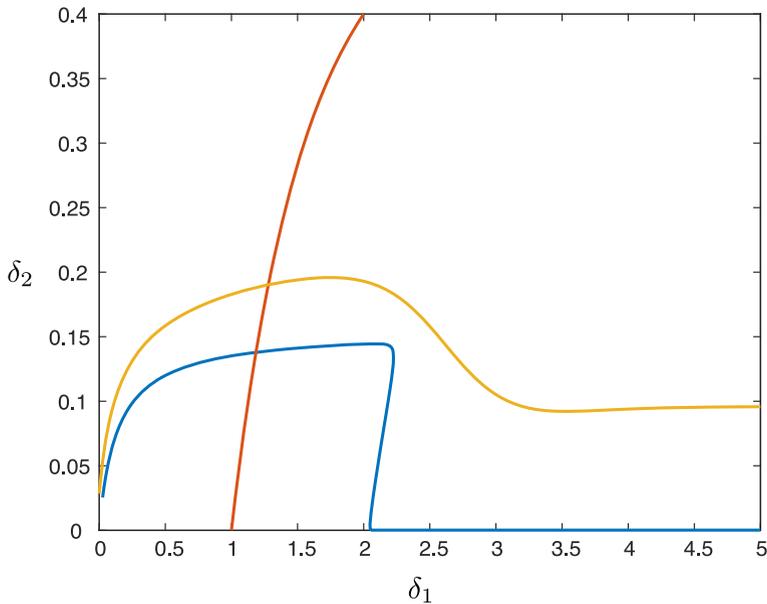
Fig. 9 Results of numerical continuation in AUTO07p (Doedel et al. 2007) for the parameter values $(a, \kappa, \delta_2, \delta_3, \rho, \varepsilon) = (0.1, 0.1, 0.1, 70, 1.0, 0.0063)$ for values of $\delta_1 \in (0.05, 15)$: wave speed c versus δ_1 (left), $\lambda_{c,2}$ versus δ_1 (right)
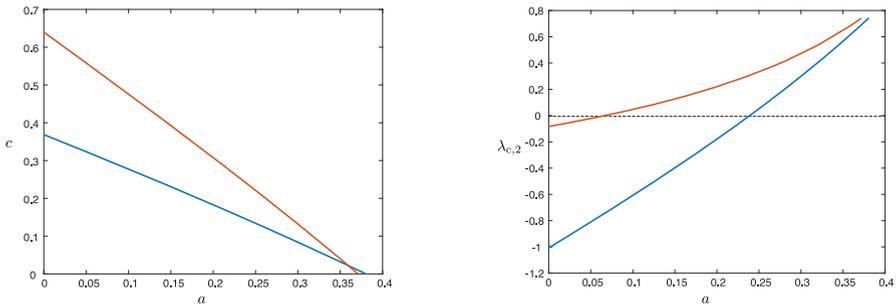
Fig. 10 Results of numerical continuation for the parameter values $(\kappa, \delta_2, \delta_3, \rho, \varepsilon) = (0.1, 0.1, 70, 1.0, 0.0063)$ for a range of a-values for $\delta_1 = 0.6$ (blue) and $\delta_1 = 12.5$ (red): wave speed c versus a (left), $\lambda_{c,2}$ versus a (right)

Our mathematical analysis and numerical simulations naturally lead to a number of biological insights, some of which we now highlight. We showed that the speed of invasion, and the probability of an acellular gap being formed, both increase as δ_1 increases. As this parameter is a measure of the negative impact of lactic acid on normal cells, this result makes intuitive sense. Furthermore, the stronger the Allee effect on the tumor cells, the slower the invasion speed of these cells, a result that also aligns with our intuition. Our study of the front instabilities showed that in such cases (strong Allee effect), the front undergoes a bifurcation that initiates the formation of growing 'fingers', resulting in an irregular morphology, while in the case of a weak Allee effect, we predict that the waves will move faster and the initial bifurcation has a milder effect and drives the development of (moving) 'cusps' in the front morpholgy, similar to that observed in the experimental results of Gatenby and Gawslinski (1996).

Note that in our model, the instability of the invasion tumor cell front is an emergent property of the system which does not require phenotypic heterogeneity within the tumor cell population or spatial heterogeneity within the system (these are often assumed to be the cases for the break-up of an invading front). However, in reality, tumors typically are very heterogeneous and the extracellular matrix (ECM)

Fig. 11 Results of numerical continuation of the curve $\lambda_{c,2} = 0$ for the parameter values $(a, \kappa, \delta_3, \rho) = (0.1, 0.1, 70, 1.0)$ in the (δ_1, δ_2)-plane for $\varepsilon = 0.0063$ (yellow) and $\varepsilon = 10^{-5}$ (blue). Below each curve we have $\lambda_{c,2} < 0$, while $\lambda_{c,2} > 0$ above. Plotted in red is the malignant/benign boundary $\delta_1 V_+ = 1$

through which they move is not spatially homogeneous. Possible future avenues of research would be to extend our present work to include these complications. Again, there is a strong similarity between cancer research and ecology (cf. Korolev et al. (2014)), in which understanding the impact of spatial heterogeneities also is a central issue (cf. Bastiaansen and Doelman (2019) and the references therein). In fact, through the link with ecology, another promising (and challenging) line of research emerges: like in ecology, interfaces between different states—bare soil/vegetated or normal/tumorous—are typically curved, not flat (as assumed here). Thus, it is necessary to extend the current approach to curved interfaces—see Byrnes et al. (2023) for some first steps in that direction in the ecological setting. Note that there also is an important distinction between ecosystem and tumor interfaces: the former typically are within two-dimensional domains (the surface of a terrain), while the latter are intrinsically three-dimensional: in combination with the local curvatures, this additional freedom may for instance have a significant impact on the nature of the protrusions initiated by the fingering instability.

From the modeling point of view, there are also various promising future research directions. For example, Strobl et al. (2020) presents a model of cancer cell invasion in which there are two different tumor cell phenotypes, one producing lactic acid and the other producing proteins that degrade the ECM, considered as a barrier to invasion. They show how different phenotypic spatial structures arise in the invading front depending on the inter-cellular competition dynamics between the two cancer cell phenotypes. More recently, Crossley et al. (2024) present a model based on volume-

filling, in which one cancer cell phenotype proliferates, while the other degrades the matrix (an example of the well-known "go-or-grow" hypothesis). Analysis of this model also gives rise to different phenotypically structured invading fronts, depending on parameter values. Both of these studies were carried out in one spatial dimension and it would be interesting to see what structures, in both physical and phenotypic space, they exhibit when considered in two (or three) spatial dimensions. A further modelling complication to address is that, while these models consider the ECM as a barrier to cancer cell invasion, the ECM also enables cell invasion through providing a "scaffold" to which cells can attach and move. Understanding in detail how this dual property of the ECM affects tumor invasion is an open question.

A Stability of steady states

We consider

$$
\begin{aligned}
U_\tau &= F(U, W) , \\
V_\tau &= G(U, V, W) + \nabla \cdot ((1 + \kappa - U)\nabla V) , \\
W_\tau &= H(V, W) + \frac{1}{\varepsilon^2} \Delta W ,
\end{aligned}
$$

where F, G, H are as in (3.2). Linearizing about a steady state $(U, V, W) = (U_0, V_0, W_0) + (\bar{u}, \bar{v}, \bar{w})e^{i(\ell_1 x + \ell_2 y) + \lambda t}$, we obtain the linearized system

$$
\lambda \begin{pmatrix} \bar{u} \\ \bar{v} \\ \bar{w} \end{pmatrix} = \begin{pmatrix} F_u & 0 & F_w \\ 0 & -(1 + \kappa - U_0)(\ell_1^2 + \ell_2^2) + G_v & G_w \\ 0 & H_v & -\frac{1}{\varepsilon^2}(\ell_1^2 + \ell_2^2) + H_w \end{pmatrix} \begin{pmatrix} \bar{u} \\ \bar{v} \\ \bar{w} \end{pmatrix} ,
\tag{A.1}
$$

where $F_u := \frac{\partial F}{\partial u}(U_0, V_0, W_0)$, etc. The steady state is stable if all eigenvalues satisfy $\mathrm{Re}(\lambda) < 0$ for all $\ell_1, \ell_2 \in \mathbb{R}$. From this we see that a necessary condition is $F_u < 0$, from which we immediately obtain that the steady state P_1 is always unstable, while P_3^+ is unstable if $\delta_1 V^+ > 1$ and P_4^+ is unstable if $\delta_1 V^+ < 1$.

The stability of the remaining steady states is determined by the lower right 2×2 block eigenvalue problem

$$
\lambda \begin{pmatrix} \bar{v} \\ \bar{w} \end{pmatrix} = \begin{pmatrix} -(1 + \kappa - U_0)(\ell_1^2 + \ell_2^2) + G_v & G_w \\ H_v & -\frac{1}{\varepsilon^2}(\ell_1^2 + \ell_2^2) + H_w \end{pmatrix} \begin{pmatrix} \bar{v} \\ \bar{w} \end{pmatrix} ,
\tag{A.2}
$$

which, following Carter et al. (2023), §2.1 are stable for $0 < \varepsilon \ll 1$, provided the conditions

$$
G_v < 0, \qquad G_v + H_w < 0, \qquad G_v H_w - G_w H_v > 0 ,
\tag{A.3}
$$
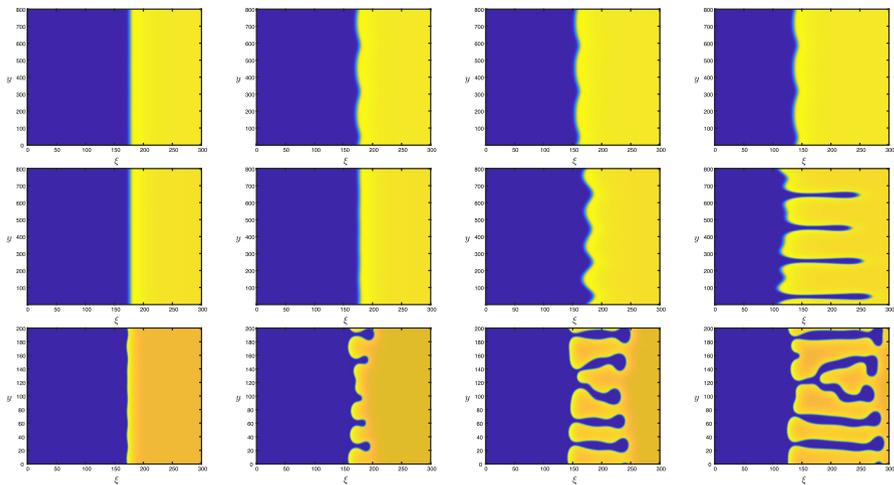
Fig. 12 Results of direct numerical simulations exhibiting different manifestations of the long wavelength instability. The simulations were performed in a co-moving frame corresponding to the wave speed of the initial front profile (so that in the absence of any instability, the fronts would appear stationary), with Neumann boundary conditions in ξ, and periodic boundary conditions in y. Finite differences were used for spatial discretization, and MATLAB's ode15s routine was used for time stepping. The corresponding v-profile is depicted, where yellow indicates high density of tumor cells, and blue depicts low density of tumor cells. (First row) Simulation for the parameter values $(a, \kappa, \delta_1, \delta_2, \delta_3, \rho, \varepsilon) = (0.25, 0.1, 12.5, 0.1, 70.0, 1.0, 0.0063)$ at the times $t = 5000, 10000, 15000, 20000$ from left to right, with wave speed $c = 0.2211$. (Second row) Simulation for the parameter values $(a, \kappa, \delta_1, \delta_2, \delta_3, \rho, \varepsilon) = (0.35, 0.1, 12.5, 0.1, 70.0, 1.0, 0.0063)$ at the times $t = 10000, 20000, 30000, 40000$ from left to right, with wave speed $c = 0.0401$. (Third row) Simulation for the parameter values $(a, \kappa, \delta_1, \delta_2, \delta_3, \rho, \varepsilon) = (0.25, 0.05, 11.5, 3, 1, 15, 0.05)$ at the times $t = 250, 350, 450, 550$ from left to right, with wave speed $c = 0.3296$. In each of the three simulations, initial conditions were constructed by trivially extending the 1D-stable profiles from Fig. 8 (rows 2 through 4) in the y-direction and adding a small amount of positive noise

are satisfied. Employing these conditions, a short computation shows that P_2 is stable, P_3^+ is stable if $\delta_1 V^+ < 1$ and P_4^+ is stable if $\delta_1 V^+ > 1$, and the remaining steady states are unstable.

Data Availability Simulation data and codes generated during the current study are available from the corresponding author on reasonable request.

Declarations

Conflict of interest The authors declare that they have no conflict of interest.

References

Anderson AR, Quaranta V (2008) Integrative mathematical oncology. Nat Rev Cancer 8(3):227–234

Bastiaansen R, Doelman A (2019) The dynamics of disappearing pulses in a singularly perturbed reaction-diffusion system with parameters that vary in time and space. Phys D Nonlinear Phenomena 388:45–72

Byrnes E, Carter P, Doelman A, Liu L (2023) Large amplitude radially symmetric spots and gaps in a dryland ecosystem model. J Nonlinear Sci 33(6):107

Carter P (2024) A stabilizing effect of advection on planar interfaces in singularly perturbed reaction-diffusion equations. SIAM J Appl Math 84(3):1227–1253

Carter P, Doelman A, Lilly K, Obermayer E, Rao S (2023) Criteria for the (in)stability of planar interfaces in singularly perturbed 2-component reaction–diffusion equations. Phys D Nonlinear Phenomena 444:133596

Chaplain M, Ganesh M, Graham I (2001) Spatio-temporal pattern formation on spherical surfaces: numerical simulation and application to solid tumour growth. J Math Biol 42:387–423

Crossley RM, Painter KJ, Lorenzi T, Maini PK, Baker RE (2024) Phenotypic switching mechanisms determine the structure of cell migration into extracellular matrix under the 'go-or-grow' hypothesis. Math Biosci, 109240

Davis PN, van Heijster P, Marangell R, Rodrigo MR (2022) Traveling wave solutions in a model for tumor invasion with the acid-mediation hypothesis. J Dyn Different Equ 34(2):1325–1347

Doedel EJ, Champneys AR, Dercole F, Fairgrieve TF, Kuznetsov YA, Oldeman B, Paffenroth R, Sandstede B, Wang X, Zhang C (2007) Auto-07p: continuation and bifurcation software for ordinary differential equations

Fasano A, Herrero M, Rodrigo M (2009) Slow and fast invasion waves in a model of acid-mediated tumour growth. Math Biosci 220:45–56

Fernandez-Oto C, Tzuk O, Meron E (2019) Front instabilities can reverse desertification. Phys Rev Lett 122(4):048101

Gallay T, Mascia C (2022) Propagation fronts in a simplified model of tumor growth with degenerate cross-dependent self-diffusivity. Nonlinear Anal Real World Appl 63:103387

Gatenby RA, Gawlinski ET (1996) A reaction-diffusion model of cancer invasion. Cancer Res 56(24):5745–5753

Gerlee P, Altrock P, Malik A, Krona C, Nelander S (2022) Autocrine signaling can explain the emergence of allee effects in cancer cell populations. PLoS Computation Biol 18(3):e1009844

Holder AB, Rodrigo MR, Herrero MA (2014) A model for acid-mediated tumour growth with nonlinear acid production term. Appl Math Comput 227:176–198

Johnson K, Howard G, Mo W, Strasser M, Ernesto E, Lima B, Huang S, Brock A (2019) Cancer cell population growth kinetics at low densities deviate from the exponential growth model and suggest an allee effect. PLoS Biol 17(8):e3000399

Katsaounis D, Harbour N, Williams T, Chaplain M, Sfakianakis N (2024) A genuinely hybrid, multiscale 3d cancer invasion and metastasis modelling framework. Bull Math Biol 86:64

Korolev KS, Xavier JB, Gore J (2014) Turning ecology and evolution against cancer. Nat Rev Cancer 14(5):371–380

Krupa M, Szmolyan P (2001) Extending slow manifolds near transcritical and pitchfork singularities. Nonlinearity 14(6):1473

Lowengrub J, Frieboes H, Jin F, Chuang Y, Li X, Macklin P, Wise S, Cristini V (2010) Nonlinear modelling of cancer: bridging the gap between cells and tumours. Nonlinearity 23:R1–R91

Martin N, Gaffney E, Gatenby R, Maini P (2010) Tumour–stromal interactions in acid-mediated invasion: a mathematical model. J Theoret Biol 267:461–470

McLennan R, McKinney M, Teddy J, Morrison J, Kasemeier-Kulesa J, Ridenour D, Manthe C, Giniunaite R, Robinson M, Baker R, Maini P, Kulesa P (2020) Neural crest cells bulldoze through the microenvironment using aquaporin 1 to stabilize filopodia. Development 147:dev185231

Perumpanani A, Sherratt J, Norbury J, Byrne H (1996) Biological inferences from a mathematical model for malignant invasion. Invasion Metastasis 16(4–5):209–2021

Sewalt L, Harley K, van Heijster P, Balasuriya S (2016) Influences of allee effects in the spreading of malignant tumours. J Theoret Biol 394:77–92

Strobl M, Krause A, Damaghi M, Gillies R, Anderson A, Maini P (2020) Mix and match: phenotypic coexistence as a key facilitator of cancer invasion. Bull Math Biol 82:15

Turner S, Sherratt JA (2002) Intercellular adhesion and cancer invasion: a discrete simulation using the extended potts model. J Theoret Biol 216(1):85–100

Verkman A, Hara-Chikuma M, Papadopoul M (2008) Aquaporins—new players in cancer biology. J Mol Med 86:523–529

Wodarz D, Komarova N (2014) Dynamics of cancer: mathematical foundations of oncology. World Scientific, Singapore